J. Shanghai Jiao Tong Univ. (Sci.), 2022
https://doi.org/10.1007/s12204-022-2409-6

Strength Optimization and Prediction of Cemented Tailings Backfill Under Multi-Factor Coupling

HU Yafei (胡亚飞), *LI Keqing* (李克庆), *HAN Bin** (韩 斌), *JI Kun* (吉 坤)
(School of Civil and Resource Engineering; Key Laboratory of Ministry of Education for High-Efficient Mining and Safety of Metal Mines, University of Science and Technology Beijing, Beijing 100083, China)

Abstract: In order to solve the problem of strength instability of cemented tailings backfill (CTB) under low temperature environment ($\leqslant 20\,^{\circ}\mathrm{C}$), the strength optimization and prediction of CTB under the influence of multiple factors were carried out. The response surface method (RSM) was used to design the experiment to analyze the development law of backfill strength under the coupling effect of curing temperature, sand-cement ratio and slurry mass fraction, and to optimize the mix proportion; the artificial neural network algorithm (ANN) and particle swarm optimization algorithm (PSO) were used to build the prediction model of backfill strength. According to the experimental results of RSM, the optimal mix proportion under different curing temperatures was obtained. When the curing temperature is 10—15 °C, the best mix proportion of sand-cement ratio is 9, and the slurry mass fraction is 71%; when the curing temperature is 15—20 °C, the best mix proportion of sand-cement ratio is 8, and the slurry mass fraction is 69%. The ANN-PSO intelligent model can accurately predict the strength of CTB, its mean relative estimation error value and correlation coefficient value are only 1.95% and 0.992, and the strength of CTB under different mix proportion can be predicted quickly and accurately by using this model.

Key words: cemented tailings backfill (CTB), response surface method (RSM), multi-factor coupling, strength optimization, intelligent prediction model
CLC number: TD 853 **Document code:** A

0 Introduction

Tailings is a solid mineral waste formed after dewatering of tailings slurry discharged from beneficiation plant. It is currently one of the bulk solid wastes with the largest output and the lowest comprehensive utilization rate in China[1-3]. Through scientific research, the tailings have been successfully used to fill the underground goaf[4-7]. Due to the extremely fine particles of the tailings, the strength of cemented tailings backfill (CTB) is unstable. A large number of laboratory tests are often needed to study the best filling mix proportion. In addition, mines located in high-cold areas are affected by the low temperature environment, which makes the strength of CTB be difficult to meet the requirements[8-10]. Therefore, exploring the influence of different factors on the strength of CTB, and conducting research on optimization and prediction of the strength of CTB are of great significance to realize low-cost and high-efficiency applications of CTB while ensuring the strength requirements.

The related scholars have carried out a lot of research work on CTB. Li et al.[11] studied the influence of solid content, cement/tailings ratio, and curing time on the strength of CTB, and found that these three factors had a positive impact on the strength of CTB within the scope of the test; that is, the larger the corresponding factor value, the higher the strength. Yin et al.[12] found that the cement content and slurry mass fraction were the main factors affecting the early strength, and optimized the mix proportion by subjective weight method. Qi et al.[13] carried out the research on the application of artificial intelligence in backfill mining, took the cement-tailings ratio, solid content and curing time as the influencing factors, and used the genetic programming method (GP) to successfully realize the high-precision prediction of the backfill strength. Zhang et al.[14] studied the influence of cement sand ratio, mass fraction and curing age on the performance of CTB, and then optimized the mix proportion and put forward the optimal mix proportion. Qi et al.[15] summarized the application status of artificial intelligence model in the strength prediction of backfill. In

Received: 2021-01-11 **Accepted:** 2021-03-02
Foundation item: the National Key Technology Research and Development Program of China (Nos. 2018YFC1900603 and 2018YFC0604604)
***E-mail:** 499310871@qq.com

the strength prediction of single tailings filling material, the artificial intelligence method is mainly the artificial neural network learning algorithm (ANN). In recent years, hybrid methods of swarm intelligence optimization algorithm and artificial intelligence algorithm have appeared one after another. In addition, studies have shown that the curing temperature has a significant impact on the strength of CTB, and low temperature will cause the strength of CTB to develop slowly[16-20]. The above research reveals the mechanism of different factors on the strength of CTB. However, there is no in-depth analysis on the strength development of backfill under the coupling of different factors, which cannot provide guidance for the safe and efficient application of CTB in mines in alpine regions.

In this study, the response surface method of Box-Behnken function in Design-Expert software (RSM-BBD) was used to optimize the experimental design, and the regression model of the strength of CTB with different curing ages was established to study the influence of the interaction coupling of different mix proportion (lime sand ratio and slurry mass fraction) and curing temperature on the strength of CTB. Based on the experimental results, the ANN-particle swarm optimization (PSO) high-precision intelligent prediction model was constructed to rapidly predict the strength of CTB with different mix proportion under different curing temperatures. The research results are of great significance to the efficient application of CTB in cold mining area.

1 Experimental Materials, Schemes and Results

1.1 Experimental Materials

The cementing material used in the experiment is type 42.5 ordinary portland cement, which is the common type of binder used for preparing CTB in practices. The tailings were taken from a gold mine in Jilin Province, China, and its main chemical composition is SiO_2, which belongs to inert material with stable properties and can be used as filling material. The contents of main chemical elements in tailings are shown in Table 1. The density of tailings is 2.71 g/cm^3, the median particle size ($D50$) is only 40 μm, and the particle size less than 75 μm accounts for about 85%, which belongs to ultra-fine tailings. The particle nonuniformity coefficient ($C_u = d_{60}/d_{10} = 10.7$) is more than 10, indicating the grading of full tailings is good and suitable as filling aggregate. The particle size composition tested by standard wet sieving and laser particle size analysis is shown in Fig. 1.

1.2 Experimental Schemes

To study the variation law of CTB uniaxial compressive strength (UCS) under multi-factor coupling, RSM-BBD was used to optimize the experimental design[21-25]. The influences of single factor and its interaction coupling on CTB strength were analyzed.

Table 1 Chemical composition of the tailings

Component	Mass fraction/%	Component	Mass fraction/%
SiO_2	66.91	Al_2O_3	16.73
CaO	5.72	SO_3	0.90
MgO	5.39	MnO	0.15
Fe_2O_3	2.26	Others	1.94

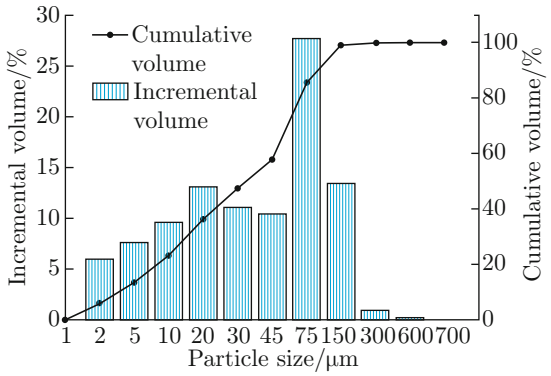

Fig. 1 Particle size composition of tailings

The freezing period of a certain gold mine in Jilin Province lasts as long as 6 months. The average temperature in the underground mine is about 10 °C in winter and no less than 20 °C in summer. The change of environment temperature has an adverse effect on the strength development of the CTB, so it is necessary to consider the effect of curing temperature on the strength of the CTB when studying the mix proportion. Based on this, we took sand-cement ratio, slurry mass fraction and curing temperature as independent variables, which were expressed by X_1, X_2 and X_3 respectively. We took 7 d, 14 d and 28 d compressive strength of CTB as response value (The test was conducted at room temperature, and the temperature has no effect on the strength of CTB during the test), which were expressed by Y_1, Y_2 and Y_3 respectively. The coupling effect of various factors on backfill strength is studied. According to a large number of exploratory tests in early stage, when the mass fraction of filling slurry is 65%—75%, and the sand-cement ratio is 6—10, the strength and fluidity of CTB can meet the requirements, and the temperature of the underground mine is basically maintained at 10—20 °C. The factors and levels of RSM-BBD test are shown in Table 2.

Table 2 RSM-BBD experimental factors and levels

Level coding	Sand-cement ratio (X_1)	Slurry mass fraction (X_2)/%	Curing temperature (X_3)/°C
−1	6	65	10
0	8	70	15
1	10	75	20

1.3 Experimental Results

Based on the central composite experiment design, Box-Behnken module in Design-Expert software was used to automatically generate 17 groups of experiments, as shown in Table 3 (For convenience of comparison, the predicted values based on the following strength model are added to the table).

Table 3 Experimental results of RSM-BBD

Serial number	Factor			Experimental value/MPa			Predicted value/MPa		
	X_1	X_2	X_3	Y_1	Y_2	Y_3	Y_1^*	Y_2^*	Y_3^*
1	6	70	20	1.61	2.15	2.12	1.65	2.20	2.28
2	8	70	15	1.05	1.42	1.68	1.04	1.42	1.70
3	8	65	20	0.42	0.87	1.12	0.33	0.82	1.04
4	8	70	15	1.04	1.42	1.71	1.04	1.42	1.70
5	8	75	10	0.9	2.28	2.95	0.99	2.33	3.03
6	8	75	20	2.19	2.83	3.45	2.25	2.83	3.45
7	6	70	10	0.82	2.03	1.95	0.82	2.03	2.03
8	10	65	15	0.29	0.63	0.82	0.39	0.68	0.98
9	6	75	15	2.43	3.54	4.47	2.33	3.49	4.31
10	10	70	10	0.41	0.93	1.11	0.37	0.88	0.95
11	8	70	15	1.03	1.40	1.67	1.04	1.42	1.69
12	10	70	20	0.92	1.26	1.32	0.92	1.26	1.24
13	8	70	15	1.06	1.43	1.69	1.04	1.42	1.69
14	8	70	15	1.03	1.42	1.70	1.04	1.42	1.69
15	6	65	15	0.52	1.25	1.37	0.57	1.25	1.29
16	8	65	10	0.27	0.78	0.91	0.21	0.78	0.91
17	10	75	15	1.39	1.99	2.41	1.34	1.99	2.49

2 Analysis and Discussion

2.1 Construction and Verification of CTB Strength Model

Design-Expert was used to perform multivariate nonlinear fitting of the experimental values of different curing ages, and established a regression model of the relationship between compressive strength and sand-cement ratio, slurry mass fraction, and curing temperature:

$$Y^* = a + \sum_{j=1}^{m} b_j x_j + \sum_{k<j} b_{kj} x_k x_j + \sum_{j=1}^{m} b_{jj} x_j^2, \quad (1)$$

where, Y^* is the response value of the measured value; a is a constant term; b_j, b_{kj} and b_{jj} are the regression coefficients of the primary, secondary and cross terms, respectively; m is the number of factors.

The 7 d, 14 d and 28 d compressive strength models of CTB are as follows:

(1) UCS at 7 d curing age:

$$\left.\begin{aligned} Y_1^* = {} & 2.8+1.153X_1-0.211X_2-0.485X_3- \\ & 0.02X_1X_2-0.007X_1X_3+0.011X_2X_3+ \\ & 0.014X_1^2+0.002X_2^2-0.006X_3^2 \\ R^2 = {} & 0.980 \end{aligned}\right\}. \quad (2)$$

(2) UCS at 14 d curing age:

$$\left.\begin{aligned} Y_2^* = {} & 37.97+0.615X_1-1.195X_2-0.344X_3- \\ & 0.023X_1X_2+0.005X_1X_3+0.0046X_2X_3+ \\ & 0.042X_1^2+0.011X_2^2+0.00024X_3^2 \\ R^2 = {} & 0.997 \end{aligned}\right\}. \quad (3)$$

(3) UCS at 28 d curing age:

$$\left.\begin{aligned} Y_3^* = {} & 73.2+2.172X_1-2.483X_2-0.049X_3- \\ & 0.038X_1X_2+0.001X_1X_3+0.003X_2X_3+ \\ & 0.012X_1^2+0.021X_2^2-0.0045X_3^2 \\ R^2 = {} & 0.977 \end{aligned}\right\}, \quad (4)$$

where R^2 is the determination coefficient.

To analyze whether the established strength model is effective, variance analysis of the above regression equation was carried out, as shown in Table 4. The P value of the strength model built in this paper is less than 0.000 1, which is extremely significant, indicating that the model has high reliability. The signal-to-noise ratio (SNR) is greater than 4, which further proves the reliability of the model. The adjustment determination coefficient (R_a^2) and R^2 of the model approach to 1, indicating that the model fits well. F =

$77.72 > F_{0.05}(3,13) = 3.41$, indicating that the model is significant and has statistical significance, which can better reflect the relationship between the compressive strength of CTB and the various influencing factors. Figure 2 shows the comparison between the strength value of backfill calculated based on the strength model and the experimental value. The experimental value is in good agreement with the predicted value, indicating that the strength model is effective. Therefore, the regression model can be used to replace the experimental data to carry out the correlation analysis of the influence of various factors on the strength of CTB.

Table 4 Variance analysis of RSM-BBD experiment results

Source of variation	Sum of squares			Mean square			F value			P value		
	Y_1	Y_2	Y_3	Y_1	Y_2	Y_3	Y_1	Y_2	Y_3	Y_1	Y_2	Y_3
Model	5.93	9.35	14.49	0.66	1.04	1.61	86.66	536.68	77.72	< 0.000 1	< 0.000 1	< 0.000 1
X_1	0.70	2.16	2.26	0.70	2.16	2.26	92.29	1 117.11	108.98	< 0.000 1	< 0.000 1	< 0.000 1
X_2	3.66	6.32	10.26	3.66	6.32	10.26	480.89	3 263.23	495.25	< 0.000 1	< 0.000 1	< 0.000 1
X_3	0.94	0.15	0.15	0.94	0.15	0.15	123.35	76.69	7.17	< 0.000 1	< 0.000 1	0.031 7
X_1X_2	0.16	0.22	0.57	0.16	0.22	0.57	21.56	111.66	27.51	0.002 4	< 0.000 1	0.001 2
X_1X_3	0.02	0.01	0.01	0.02	0.01	0.01	2.58	5.69	0.02	0.152 5	0.048 4	0.893 4
X_2X_3	0.32	0.05	0.02	0.32	0.05	0.02	42.71	27.32	1.01	0.000 3	0.001 2	0.347 3
X_1^2	0.01	0.12	0.01	0.01	0.12	0.01	1.69	61.74	0.46	0.234 8	0.000 1	0.520 1
X_2^2	0.02	0.30	1.18	0.02	0.30	1.18	2.01	153.85	57.09	0.199 3	< 0.000 1	0.000 1
X_3^2	0.10	0.01	0.05	0.10	0.01	0.05	13.69	0.078	2.57	0.007 7	0.787 7	0.152 8

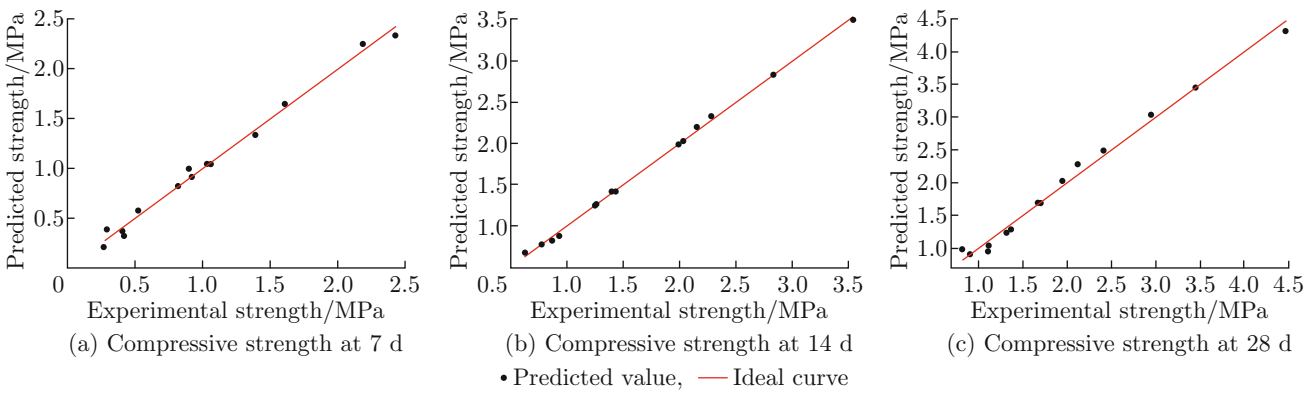

Fig. 2 Comparison of experimental value and predicted value of backfill strength

2.2 Single Factor on Strength of CTB

According to the variance analysis of strength regression model, the curing temperature has a very significant effect on the early strength of CTB ($P < 0.01$), and it has a significant impact on the strength of the middle and late stages ($P < 0.05$). The slurry mass fraction and sand-cement ratio have a extremely significant impact on the compressive strength of the CTB during the whole curing period ($P < 0.01$).

2.2.1 *Curing Temperature on Strength of CTB*

The slurry mass fraction is fixed at 70% and the sand-cement ratio is fixed at 8. The influence of curing temperature on the strength of CTB is shown in Fig. 3. With the decrease of curing temperature, the rate of decrease in the strength of the CTB increases. When the curing temperature is lower than 15 °C, the strength of CTB decreases greatly. The transverse comparison shows that the curing temperature has obvious influence on the early strength of the CTB, but the influence on the middle and late strength is relatively weak. When the curing temperature is reduced from 20 °C to 10 °C, the 14 d and 28 d strengths of the CTB are reduced by 14.6% and 16.8% respectively. While the 7 d strength of the CTB is reduced by 55.7%, and the reduction range of the 7 d strength is about three times of those of the 14 d and 28 d strengths. At the early stage of curing, the hydration reaction rate is slow and the amount of cementitious material is less. Under the action of low temperature, the hydration reaction rate is further reduced, the setting time of slurry

is prolonged, and the strength of CTB is greatly reduced. After the backfill is cured to the middle and late stages, most of the cement in the backfill takes part in the hydration reaction and generates more cementitious materials, which has a certain strength. The low temperature only affects a small part of the materials that have not completed the hydration reaction. Therefore, the strength of the CTB in the middle and later stages is relatively less affected by temperature.

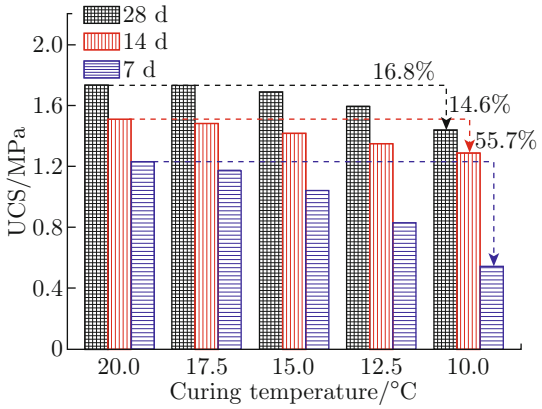

Fig. 3 Effect of curing temperature on strength

2.2.2 *Sand-Cement Ratio on Strength of CTB*

The slurry mass fraction is fixed at 70% and the curing temperature is fixed at 20 °C, the influence of sand-cement ratio on the strength of the CTB is shown in Fig. 4. With the increase of sand-cement ratio, the strength of CTB at different curing ages shows a significant decrease trend; when the sand-cement ratio increases from 6 to 10, the strength of 7, 14 and 28 d decreases by 44.2%, 42.6% and 45.6% respectively. The main source of the CTB strength is the C-S-H gels, $Ca(OH)_2$ crystals and Aft crystals produced by the hydration reaction. C-S-H gels are formed in the whole stage of hydration reaction, Aft crystals are mainly formed in the early stage, and $Ca(OH)_2$ crystals are mainly formed in the middle and later stages. These materials can fully fill the pores between tailings and

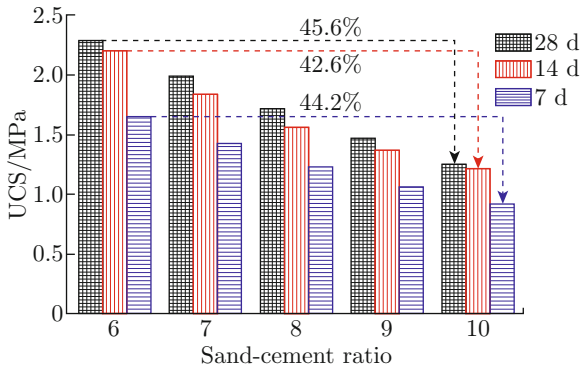

Fig. 4 Effect of sand-cement ratio on strength

connect the loose sand body into a dense cemented structure to ensure that the backfill has high strength in each curing age. The increase of sand-cement ratio means that the amount of cement used as cementitious material in the backfill becomes smaller, leading to the decrease of hydration products in each age, and the loose sand body can't be fully cemented, thus reducing the strength of backfill at each age.

2.2.3 *Slurry Mass Fraction on Strength of CTB*

The sand-cement ratio is fixed at 8, the curing temperature is fixed at 20 °C, and the influence of the slurry mass fraction on the strength of CTB is shown in Fig. 5. The strength of CTB increases with the increase of slurry mass fraction. When the slurry mass fraction is increased from 65% to 75%, the strength of 7 d, 14 d and 28 d increases by 582%, 245% and 232%, respectively, which means that the increase of slurry mass fraction is more significant to the improvement of early strength; the strength of 7 d, 14 d and 28 d increases by 0.19 MPa, 0.20 MPa and 0.24 MPa respectively when the slurry mass fraction is increased by 1%. The increase in mass fraction increases the viscosity of the filling slurry, increases the settlement resistance of the aggregate in the slurry, reduces bleeding and the layering and segregation of the aggregate, and the distribution of the aggregate is more uniform.

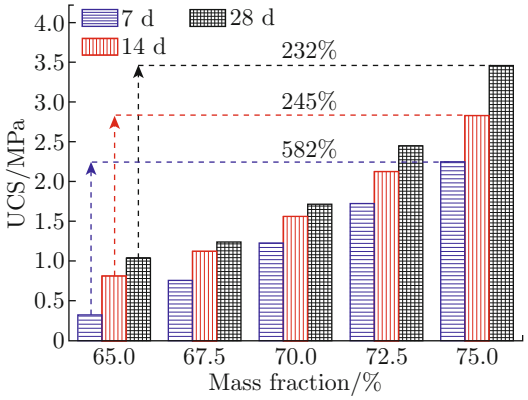

Fig. 5 Effect of mass fraction on strength

2.3 Multi-Factor Interaction and Coupling on Strength of CTB

From the analysis of variance of the strength regression model, the interactive coupling between mass fraction and curing temperature has a significant impact on the early strength of the backfill. The interactive coupling between mass fraction and sand-cement ratio has a significant impact on the mid-term strength of the backfill. The interactive coupling between sand-cement ratio and curing temperature It has a significant impact on the later strength of the backfill.

2.3.1 *Interaction Between Mass Fraction and Curing Temperature on Strength of CTB*

Figure 6 shows the response surface diagram and contour diagram of the 7 d strength of the backfill under the interaction of mass fraction and curing temperature, and the sand-cement ratio is a fixed factor. It can be seen from Fig. 6(a) that when the curing temperature is low, increasing the mass fraction can improve the early strength of the backfill, but the strength increase is small, and the response surface is slow. When the curing temperature is high, the early strength of the backfill can be significantly improved by increasing the mass fraction, and the response surface is steep. When the curing temperature is 10 °C, the mass fraction is increased from 65% to 75%, and the 7 d strength of the backfill is increased by 0.7 MPa. When the curing temperature is 20 °C, the strength of the backfill is increased by 1.85 MPa under the same conditions, and the improvement effect is obvious. Therefore, increasing the curing temperature is helpful to give full play to the physical characteristics of the filling slurry. From Fig. 6(b), with the increase of mass fraction and curing temperature, the spacing between strength isolines gradually narrows, indicating that the early strength of backfill can be significantly improved by the interaction of mass fraction and curing temperature.

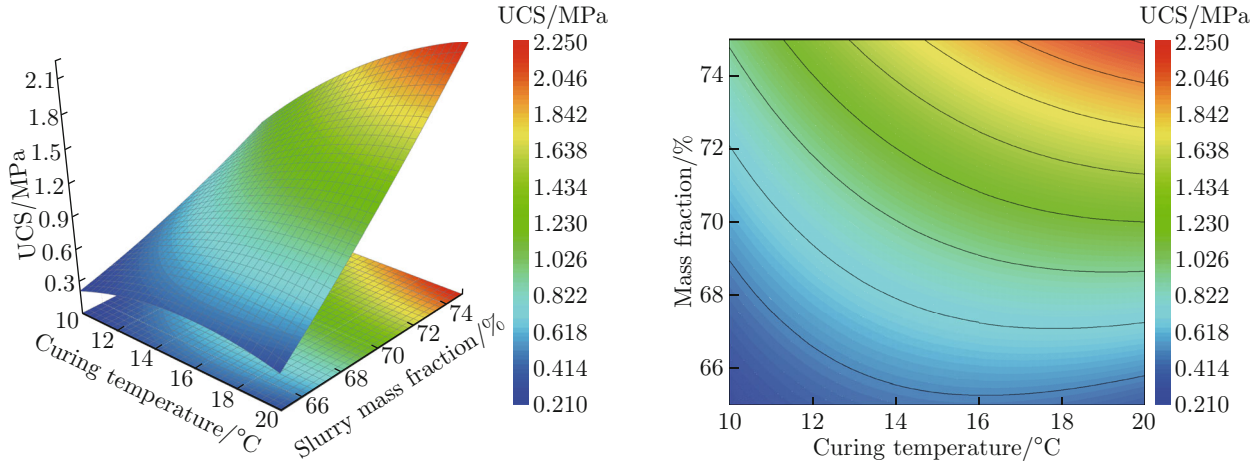

(a) Response surface (b) Contour map

Fig. 6 Influence of interaction between mass fraction and curing temperature on strength

2.3.2 *Interaction Between Sand-Cement Ratio and Mass Fraction on Strength of CTB*

Figure 7 shows the response surface diagram and contour diagram of the 14 d strength of the backfill under the interaction of mass fraction and sand-cement ratio, and the curing temperature is a fixed factor. Under the same sand-cement ratio, the strength of the backfill increases with the increase of the mass fraction, and the smaller the sand-cement ratio, the more obvious the strength increase. Under the same mass fraction, the strength of the backfill decreases with the increase of the sand-cement ratio. When the sand-cement ratio is 10 and the mass fraction is increased from 65% to 75%, the strength of the backfill is increased by 1.13 MPa. When the sand-cement ratio is 6, the strength of the backfill is increased by 2.27 MPa under the same conditions. The lower the sand-cement ratio is, the higher the cement content in the filling slurry is, and a large amount of cementitious materials are generated to fill and wrap the tailings particles in the middle of the curing period of the backfill. The increase of the slurry mass fraction means that the water content in the slurry is reduced, which is more conducive to the cementation and setting of the slurry, so it has a higher medium-term strength.

2.3.3 *Interaction Between Sand-Cement Ratio and Curing Temperature on Strength of CTB*

Figure 8 shows the response surface diagram and contour diagram of the 28 d strength of the backfill under the interaction of sand-cement ratio and curing temperature, and the mass fraction is a fixed factor. Reducing the sand-cement ratio and increasing the curing temperature can significantly improve the later strength of the backfill. The influence of sand-cement ratio on the strength of backfill is more obvious in low temperature environment than in high temperature environment. When the curing temperature is 10 °C, the sand-cement ratio is reduced from 10 to 6, and the filling strength is increased by 111.6%. When the curing temperature is 20 °C, the sand-cement ratio is reduced from 10 to 6, and the filling strength is increased by 89% That is, if the backfill wants to obtain the ideal strength at low temperature, the cement content needs to be increased. The decrease of sand-cement ratio means that the cement content in the filling slurry increases, the hydration reaction of cement at low temperature is

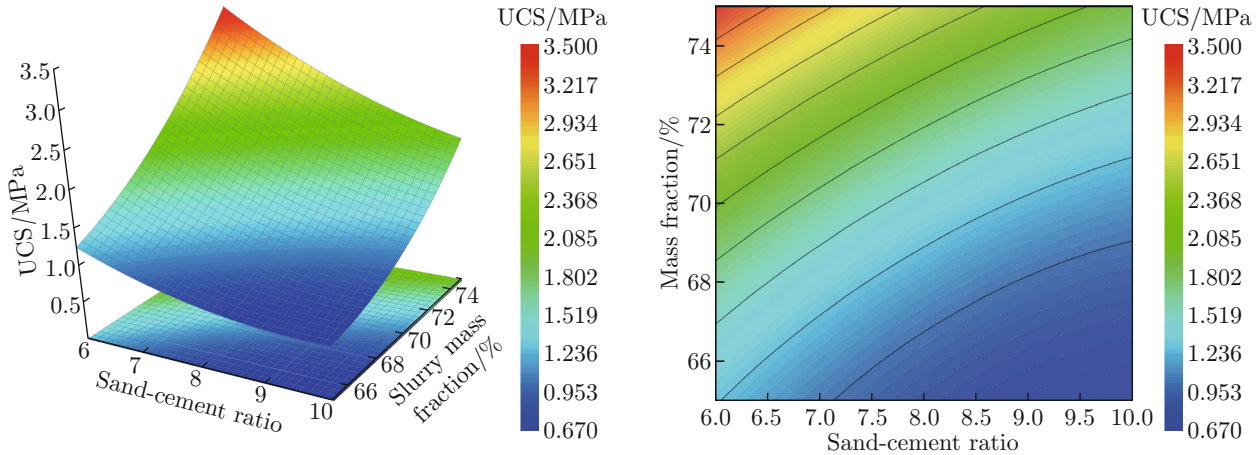

(a) Response surface (b) Contour map

Fig. 7 Influence of interaction between mass fraction and sand-cement ratio on strength

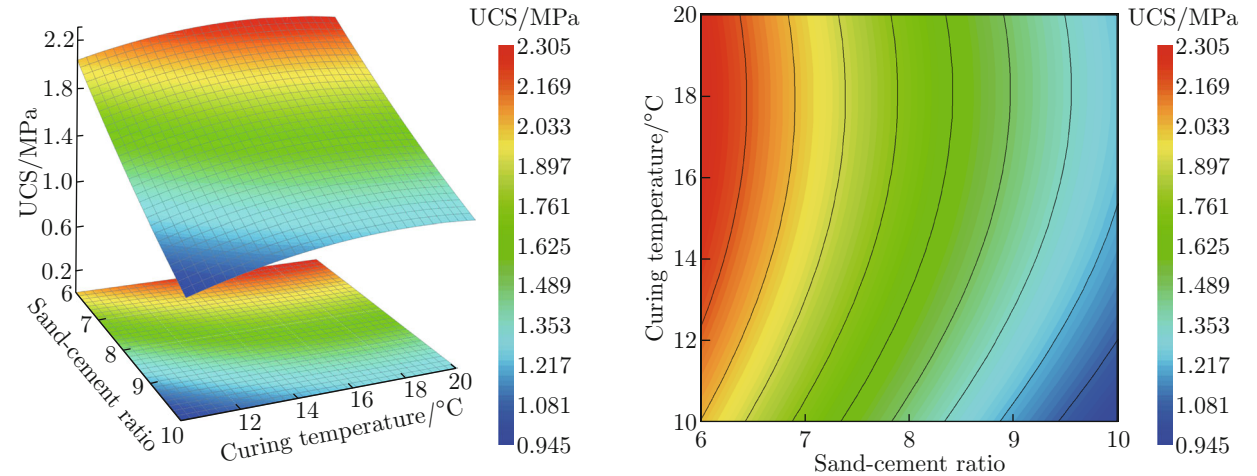

(a) Response surface (b) Contour map

Fig. 8 Influence of interaction between sand-cement ratio and curing temperature on strength

slow, and the amount of cementitious material is less, which leads to the decrease of backfill strength. The increase of curing temperature under high cement content is more conducive to the hydration reaction of cement, and the strength of backfill is significantly improved.

2.4 Strength Optimization of Backfill Based on RSM-BBD

The 7 d, 14 d and 28 d UCS requirements of CTB shall not be less than 0.8 MPa, 1.0 MPa and 1.5 MPa respectively. Considering that the underground temperature is in the range of 10—20 °C, to meet the requirements of backfill strength under different temperatures, it is necessary to select the matching mix proportion according to different underground temperatures. When the underground temperature is lower than 15 °C, adopting the mix proportion that meets the strength requirements obtained by curing at 10 °C. When the underground temperature is higher than 15 °C, adopting the mix proportion that meets the strength requirements obtained by curing at 15 °C. In this way, it can ensure that the backfill strength meets the requirements at different underground temperatures without causing waste filling materials. By using Design-Expert software to solve the strength model of backfill, the best mix proportion under the target strength can be obtained, seen in Table 5 and Fig. 9.

3 Strength Prediction of Backfill Based on ANN-PSO Model

3.1 Construction of ANN-PSO Strength Prediction Model

3.1.1 *ANN Prediction Model*

Back propagation (BP) is an efficient type of ANN[26-28]. The nonlinear relationship between input value and output value is established by training sample data. The neural network includes input layer, hidden layer and output layer. In this paper, the four factors

Table 5 Optimal mix proportion of CTB

Applicable temperature/°C	Optimum mix proportion		Mix proportion rounding	
	Sand-cement ratio	Mass fraction/%	Sand-cement ratio	Mass fraction/%
$\geqslant 15$	7.92	68.99	8.00	69.00
< 15	8.75	70.73	9.00	71.00

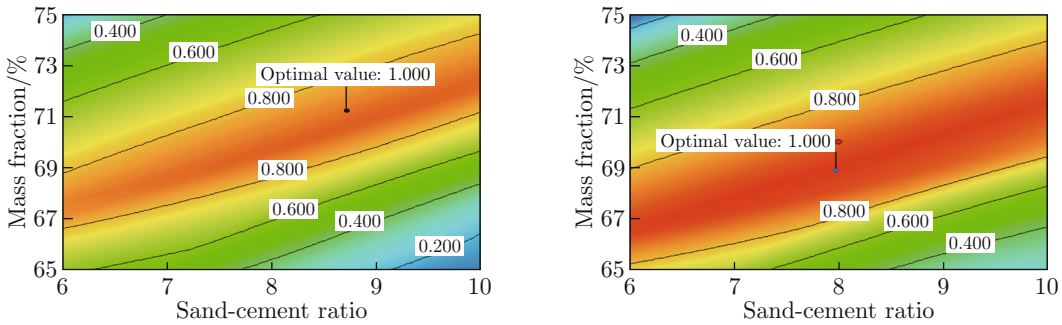

(a) Temperature is lower than 15 °C (b) Temperature is higher than 15 °C

Fig. 9 Value point of optimal mix proportion

of curing temperature, sand-cement ratio, slurry mass fraction and curing time can affect the strength of backfill, so the number of input layer neurons is 4; the output value of output layer is the compressive strength of backfill, so the output layer contains 1 neuron; the selection of the number of hidden layer neurons directly affects the prediction accuracy of the model, but it is not accurate at present[29,30]. Therefore, this paper establishes the BP neural network model of 8 different hidden layer neurons (5—12) to determine the most accurate calculation model. When BP neural network is running, the input signal is processed layer by layer from the input layer to the output layer through the hidden layer. If the expected output cannot be obtained in the output layer, the error back-propagation is turned on, and the weight and threshold value are modified according to the error, so that the predicted output is constantly close to the expected output.

In this model, Levenberg-Mrquardt algorithm is used in the input layer, and transfer functions logsig and purelin are used in the hidden layer and output layer, respectively. The training times are set at 3 000, the learning rate is taken as 0.2, and the momentum coefficient is taken as 0.7.

3.1.2 *Optimization of ANN Model by PSO Algorithm*

Due to the low precision of ANN model, PSO algorithm is considered to optimize ANN model[31-34]. PSO algorithm is a powerful global optimization algorithm, which simulates the predation behavior of birds. In PSO, each bird represents a "particle", and each particle contains two attributes: position and speed[35,36]. In this paper, the particle position represents the initial weight and threshold of the network, and the velocity represents the amplitude of the initial weight and threshold each time they are updated. The specific steps of PSO algorithm to optimize ANN initial weights and thresholds are as follows: ① The topological structure of BP neural network is established. ② Particle position and velocity initialization. Initialization is accomplished by generating a group of particles with random positions and velocities (random solutions). ③ Calculate the fitness value of particles. The fitness value is calculated by the fitness function. In this paper, the mean square error (MSE) is used as the fitness function. The smaller the MSE value is, the better the particle is. ④ Particle speed and position update. Based on this step, the better particles can be captured continuously, so as to approach the optimal particles continuously. The update formulas of particle speed (V_{d}) and position (X_{d}) are

$$V_{\mathrm{d}}(t+1) = \omega(t)V_{\mathrm{d}}(t) + c_1 r_1(P_{\mathrm{d}}(t) - X_{\mathrm{d}}(t)) + c_2 r_2(G_{\mathrm{d}}(t) - X_{\mathrm{d}}(t)), \quad (5)$$

$$X_{\mathrm{d}}(t+1) = X_{\mathrm{d}}(t) + V_{\mathrm{d}}(t+1), \quad (6)$$

where r_1 and r_2 are evenly distributed random numbers in [0, 1]; c_1 and c_2 are learning factors, which are taken as 1.8; w is inertia weight; $P_{\mathrm{d}}(t)$ is the optimal position of the particle itself; $G_{\mathrm{d}}(T)$ is the optimal position of the population; $X_{\mathrm{d}}(t)$ is the current position of the particle. The particle swarm size of PSO algorithm is 300, the particle length is 21, and the number of iterations is 100. After the iteration, the weights and thresholds of the optimal particles become the optimal initial weights and thresholds of the neural network.

3.1.3 *ANN-PSO Intelligent Prediction Model*

The ANN-PSO optimization model was constructed to predict the strength of backfill with different curing temperature and mix proportion.

3.2 Analysis of Prediction Effect of ANN-PSO Model

There are 17 groups of experiments in Table 3, but there are 5 groups of repeated experiments. Therefore, there are 13 groups of non repeated experiments in Table 3. Each group can get three strength values of 7 d, 14 d and 28 d, that is, there are 39 non repeated strength samples in Table 3. From the 39 samples of non-repetitive data of the RSM-BBD experiment, 31 samples were randomly selected as the training set and 8 samples were used as the test set, the training set was used to debug and train the ANN-PSO model, and the test set was used to evaluate the prediction performance of the model. The mean relative estimation error (MRE) and the coefficient of determination (R^2) were used to evaluate the prediction effect of the ANN-PSO model. The closer the MRE value is to 0 and the closer the R^2 value to 1, the better the prediction effect of the model is. The calculation formulas are

$$\mathrm{MRE} = \frac{1}{n}\sum_{i=1}^{n}\left|\frac{y_i - p_i}{y_i}\right| \times 100\%, \tag{7}$$

$$R^2 = 1 - \frac{\sum_{i=1}^{n}(y_i - p_i)^2}{\sum_{i=1}^{n}(y_i - \bar{y}_i)^2}, \tag{8}$$

where y_i, p_i are the experimental value and the predicted value respectively, and $\bar{y}_i$ are the average value of the experimental value.

Figure 10 shows the relationship between different numbers of hidden layer neurons and the MRE and R^2 of the test set. The MRE of the model optimized by PSO algorithm is significantly lower than that of the model without PSO optimization, with the maximum reduction value of 19.6%. At the same time, after the optimization of PSO algorithm, the goodness of fit of the model has been significantly improved, and the maximum increase of R^2 value is 0.091. The performance of the above two evaluation indexes comprehensively illustrates the effectiveness and superiority of the PSO algorithm in optimizing ANN. In addition, with the increase of the number of hidden layer neurons, the MRE value of the prediction model first decreases and then increases, and the R^2 value first increases and then decreases. The reason is that when the number of hidden layer neurons is too small, it is impossible to establish an effective mapping between input and output to express the nonlinear relationship between them. When the number of hidden layer neurons is too large, the complexity of the network will be greatly increased, which will lead to over fitting phenomenon and reduce the prediction accuracy. When the number of neurons is 9, the minimum MRE value is 1.95% and the maximum R^2 value is 0.992. At this time, the model has the best predictive performance.

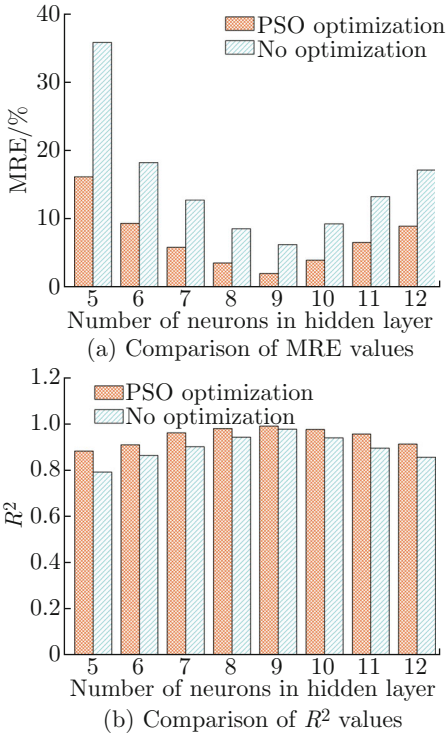

(a) Comparison of MRE values

(b) Comparison of R^2 values

Fig. 10 Prediction performance of ANN model

The network structure of the final prediction model is 4-9-1 structure, as shown in Fig. 11.

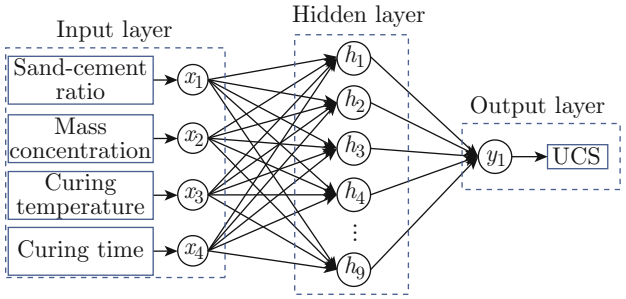

Fig. 11 Network structure of ANN model

Figure 12 shows the comparison between the strength predicted by ANN-PSO model and the experimental value. It can be seen from Figs. 12(a) and 12(c) that the predicted values of the training set and the test set are in good agreement with the experimental data, and the corresponding MRE values are 2.18% and 1.95% respectively. Figures 12 (b) and 12(d) show that the regression results of the training set and the test set are better, with R^2 values of 0.988 and 0.992 respectively. The above results comprehensively show that the model is well trained, avoids insufficient fitting and overfitting, can accurately express the nonlinear relationship between various influencing factors and compressive strength, and has a good effect on the prediction of the strength of the backfill.

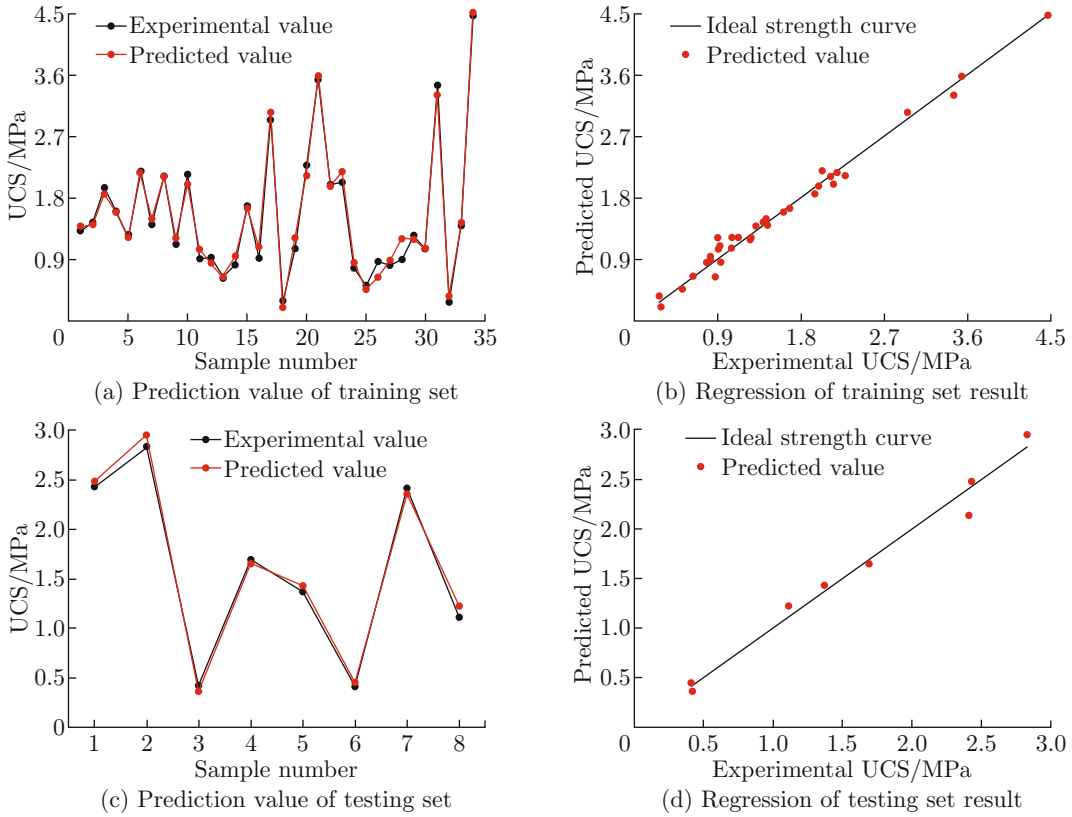

(a) Prediction value of training set
(b) Regression of training set result
(c) Prediction value of testing set
(d) Regression of testing set result

Fig. 12 Prediction performance of ANN model

3.3 Application of ANN-PSO Strength Prediction Model

The ANN-PSO model was used to predict the strength of mix proportion in Table 5, and the strength experiment of the CTB under the corresponding mix proportion was carried out to obtain the strength values of 7, 14 and 28 days to verify the accuracy of the prediction model and the rationality of the mix proportion. The results are shown in Fig. 13. The results show that the experimental values and predicted values of mix proportion in Table 5 meet the strength requirements, and the error rates of predicted values are less than 3.2% compared with the experimental values. Based on the intelligent model, the high-precision prediction of the strength of the CTB is realized. The intelligent prediction model can also be used to quickly and flexibly adjust the mix proportion according to the actual demand of filling, reduce the tedious indoor test work, and greatly improve the applicability of the filling slurry under different strength requirements. It should be noted that the intelligent model constructed in this paper is suitable for specific conditions, and its advantage over the regression model is that it can better deal with the nonlinear relationship; the accuracy of the intelligent model depends on the number of samples, and

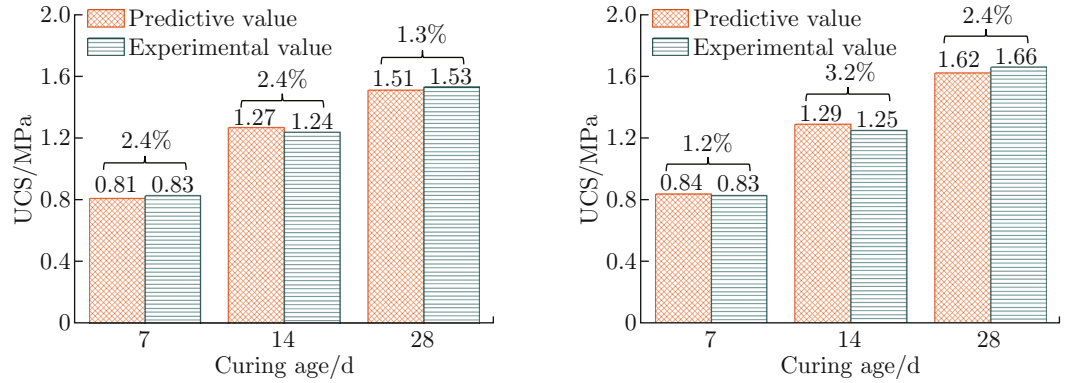

(a) Temperature is lower than 15 °C
(b) Temperature is higher than 15 °C

Fig. 13 Strength prediction of filling mix proportion

the higher the number of samples, the better the prediction accuracy of the model.

4 Conclusion

In this paper, we discussed the influence of different factors on the strength of CTB, and built an intelligent strength prediction model. The following conclusions can be made based on the research results:

(1) Based on RSM-BBD experiment, a multi-element nonlinear strength model was established with sand-cement ratio, slurry mass fraction and curing temperature as influencing factors. The P value of the strength model was very small ($P < 0.000\,1$), indicating that the model has high reliability. The minimum value of F test of the model was $F = 77.72 > 3.41$, which shows that the model is significant and statistically significant, and can better reflect the relationship between the compressive strength of CTB and the influencing factors.

(2) The influence of single factor and multi factor interaction coupling on the strength of CTB was studied. The results show that curing temperature has a significant effect on the early strength of CTB, the slurry mass fraction and the sand-cement ratio have a significant impact on the strength of CTB in the whole curing period. The interaction coupling effect of the slurry mass fraction and the curing temperature has a significant impact on the early strength of CTB. The interaction coupling effect of the slurry quality concentration and the sand-cement ratio has a significant impact on the medium-term strength of CTB. The interaction coupling effect of the sand-cement ratio and the curing temperature has a significant impact on the later strength of CTB.

(3) In this paper, the ANN-PSO intelligent strength prediction model was established, and the MRE value and R^2 value are 1.95% and 0.992 respectively, which has a good prediction effect on the strength of CTB. The mix proportion of CTB suitable for different environmental temperatures was proposed and the strength prediction was carried out. The strength error rate was less than 3.2% compared with the actual value.

Acknowledgment The authors thank Jinying Gold Mine for providing the experimental materials.

References

[1] GAO S, CUI X W, KANG S B, et al. Sustainable applications for utilizing molybdenum tailings in concrete [J]. *Journal of Cleaner Production*, 2020, **266**: 122020.

[2] LI L, JIANG T, CHEN B J, et al. Overall utilization of vanadium-titanium magnetite tailings to prepare lightweight foam ceramics [J]. *Process Safety and Environmental Protection*, 2020, **139**: 305-314.

[3] DENG H W, HE W, ZHOU K P. Heavy metals distribution in reclamation tailings and assessment of ecological risk [J]. *The Chinese Journal of Nonferrous Metals*, 2015, **25**(10): 2929-2935 (in Chinese).

[4] ZHANG Q L, WANG S, WANG X M. Influence rules of unit consumptions of flocculants on interface sedimentation velocity of unclassified tailings slurry [J]. *The Chinese Journal of Nonferrous Metals*, 2017, **27**(2): 318-324 (in Chinese).

[5] LIU B, GAO Y T, JIN A B, et al. Dynamic characteristics of superfine tailings-blast furnace slag backfill featuring filling surface [J]. *Construction and Building Materials*, 2020, **242**: 118173.

[6] ZHAO K, YU X, ZHU S T, et al. Acoustic emission investigation of cemented paste backfill prepared with tantalum-niobium tailings [J]. *Construction and Building Materials*, 2020, **237**: 117523.

[7] XU W B, CAO Y, LIU B H. Strength efficiency evaluation of cemented tailings backfill with different stratified structures [J]. *Engineering Structures*, 2019, **180**: 18-28.

[8] ZHANG S Y, REN F Y, GUO Z B, et al. Strength and deformation behavior of cemented foam backfill in subzero environment [J]. *Journal of Materials Research and Technology*, 2020, **9**(4): 9219-9231.

[9] ROSHANI A, FALL M. Rheological properties of cemented paste backfill with nano-silica: Link to curing temperature [J]. *Cement and Concrete Composites*, 2020: **114**: 103785.

[10] FANG K, FALL M. Effects of curing temperature on shear behaviour of cemented paste backfill-rock interface [J]. *International Journal of Rock Mechanics and Mining Sciences*, 2018, **112**: 184-192.

[11] LI J J, YILMAZ E, CAO S. Influence of solid content, cement/tailings ratio, and curing time on rheology and strength of cemented tailings backfill [J]. *Minerals*, 2020, **10**(10): 922.

[12] YIN S H, LIU J M, SHAO Y J, et al. Influence rule of early compressive strength and solidification mechanism of full tailings paste with coarse aggregate [J]. *Journal of Central South University*(*Science and Technology*), 2020, **51**(2): 478-488 (in Chinese).

[13] QI C C, TANG X L, DONG X J, et al. Towards intelligent mining for backfill: A genetic programming-based method for strength forecasting of cemented paste backfill [J]. *Minerals Engineering*, 2019, **133**: 69-79.

[14] ZHANG F X, KANG Z Q, XIN D F. Characteristic test and proportion study of cemented backfill in an iron mine [J]. *Mining Research and Development*, 2020, **40**(2): 38-41(in Chinese).

[15] QI C C, YANG X Y, LI G C, et al. Research status and perspectives of the application of artificial intelligence in mine backfilling [J]. *Journal of China Coal Society*, 2021, **46**(2): 688-700 (in Chinese).

[16] XU W B, LI Q L, LIU B. Coupled effect of curing temperature and age on compressive behavior, microstructure and ultrasonic properties of cemented

tailings backfill [J]. *Construction and Building Materials*, 2020, **237**: 117738.

[17] WANG Y, WU A X, WANG H J, et al. Effect of low temperature on early strength of cemented paste backfill from a copper mine and engineering recommendations [J]. *Chinese Journal of Engineering*, 2018, **40**(8): 925-930 (in Chinese).

[18] HOU C, ZHU W C, YAN B X, et al. The effects of temperature and binder content on the behavior of frozen cemented tailings backfill at early ages [J]. *Construction and Building Materials*, 2020, **239**: 117752.

[19] CHEN S M, WU A X, WANG Y M, et al. Coupled effects of curing stress and curing temperature on mechanical and physical properties of cemented paste backfill [J]. *Construction and Building Materials*, 2021, **273**: 121746.

[20] BULL A J, FALL M. Curing temperature dependency of the release of arsenic from cemented paste backfill made with Portland cement [J]. *Journal of Environmental Management*, 2020, **269**: 110772.

[21] FU Z G, QIAO D P, GUO Z L, et al. Experimental research on mix proportioning and strength of cemented hydraulic fill with waste rock and eolian sand based on RSM-BBD [J]. *Journal of China Coal Society*, 2018, **43**(3): 694-703 (in Chinese).

[22] TAO Y J, ZHU X N, TAO D P, et al. Optimization of triboelectrostatic decarbonization experiment of fly ash by Design-Expert [J]. *Journal of China Coal Society*, 2016, **41**(2): 475-482 (in Chinese).

[23] GAO Q, YANG X B, WEN Z J, et al. Optimization of proportioning of mixed aggregate filling slurry based on BBD response surface method [J]. *Journal of Hunan University* (*Natural Sciences*), 2019, **46**(6): 47-55 (in Chinese).

[24] ZHU L Y, LÜ W S, YANG P, et al. Thickening sedimentation of unclassified tailings under influence of external field based on response surface method [J]. *The Chinese Journal of Nonferrous Metals*, 2018, **28**(9): 1908-1917 (in Chinese).

[25] WU H, ZHAO G Y, CHEN Y. Multi-objective optimization for mix proportioning of mine filling materials [J]. *Journal of Harbin Institute of Technology*, 2017, **49**(11): 101-108 (in Chinese).

[26] XU M F, GAO Y T, JIN A B, et al. Prediction of cemented backfill strength by ultrasonic pulse velocity and BP neural network [J]. *Chinese Journal of Engineering*, 2016, **38**(8): 1059-1068 (in Chinese).

[27] JAHANGIR H, EIDGAHEE D R. A new and robust hybrid artificial bee colony algorithm-ANN model for FRP-concrete bond strength evaluation [J]. *Composite Structures*, 2021, **257**: 113160.

[28] RAO P S, KUMAR S, KHAN M Y. Comparison of prediction capabilities of MRR parameter using RSM and ANN for dry turning of Inconel 825 alloy using cryogenically treated tungsten carbide tool [J]. *Materials Today*: *Proceedings*, 2020. https://doi.org/10.1016/j.matpr.2020.10.163.

[29] ALONSO-MONTESINOS J, BALLESTRÍN J, LÓPEZ G, et al. The use of ANN and conventional solar-plant meteorological variables to estimate atmospheric horizontal extinction [J]. *Journal of Cleaner Production*, 2021, **285**: 125395.

[30] Chinese Forum of MATLAB. MATLAB neural network analysis of 30 cases [M]. Beijing: Beijing University of Aeronautics and Astronautics Press, 2010 (in Chinese).

[31] QI C C, CHEN Q S, FOURIE A, et al. An intelligent modelling framework for mechanical properties of cemented paste backfill [J]. *Minerals Engineering*, 2018, **123**: 16-27.

[32] RAMACHANDRAN S, JAYALAL M L, RIYAS A, et al. Application of genetic algorithm for optimization of control rods positioning in a fast breeder reactor core [J]. *Nuclear Engineering and Design*, 2020, **361**: 110541.

[33] ZHOU K P, WANG X X, GAO F. Stope structural parameters optimization based on strength reduction and ANN-GA model [J]. *Journal of Central South University* (*Science and Technology*), 2013, **44**(7): 2848-2854 (in Chinese).

[34] WU W, JI K, ZHANG P. Strength prediction of filling body based on ANN-PSO model and its engineering application [J]. *Mining Research and Development*, 2020, **40**(2): 53-57 (in Chinese).

[35] SHAO H D, DING Z Y, CHENG J S, et al. Intelligent fault diagnosis among different rotating machines using novel stacked transfer auto-encoder optimized by PSO [J]. *ISA Transactions*, 2020, **105**: 308-319.

[36] MA C, ZHAO L, MEI X S, et al. Thermal error modeling of machine tool spindle based on particle swarm optimization and neural network [J]. *Journal of Shanghai Jiao Tong University*, 2016, **50**(5): 686-695 (in Chinese).